
On the strength and disruption mechanisms of small bodies in the Solar System

Patrick Michel¹

Laboratoire Cassiopée, Observatoire de la Côte d'Azur, CNRS, Université de Nice Sophia-Antipolis, boulevard de l'Observatoire, 06300 Nice, France michel@oca.eu

Abstract

During their evolutions, the small bodies of our Solar System are affected by several mechanisms which can modify their properties. While dynamical mechanisms are at the origin of their orbital variations, there are other mechanisms which can change their shape, spin, and even their size when their strength threshold is reached, resulting in their disruption. Such mechanisms have been identified and studied, by both analytical and numerical tools. The main mechanisms that can result in the disruption of a small body are collisional events, tidal perturbations, and spin-ups. However, the efficiency of these mechanisms depends on the strength of the material constituting the small body, which also plays a role in its possible equilibrium shape. As it is often believed that most small bodies larger than a few hundreds meters in radius are gravitational aggregates or rubble piles, i.e. cohesionless bodies, a fluid model is often used to determine their bulk densities, based on their shape and assuming hydrostatic equilibrium. A representation by a fluid has also been often used to estimate their tidal disruption (Roche) distance to a planet. However, cohesionless bodies do not behave like fluids. In particular, they are subjected to different failure criteria depending on the supposed strength model. This paper presents several important aspects of material strengths that are believed to be adapted to Solar System small bodies and reviews the most recent studies of the different mechanisms that can be at the origin of the disruption of these bodies. Our understanding of the complex process of rock failure is still poor and remains an open area of research. While our knowledge has improved on the disruption mechanisms of small bodies of our Solar System, there is still a large debate on the appropriate strength models for these bodies. Moreover, material properties of terrestrial rocks or meteorites are generally used to model small bodies in space, and only space missions to some of these bodies devoted to precise in-situ analysis and sample return will allow us to determine whether those models are appropriate or need to be revised.

To be published in:
"Small Bodies in Planetary Systems".
(Mann, Nakamura, Mukai eds.)
Submitted to Lecture Notes in Physics series by Springer
Funded by the 21st Century COE Program
"Origin and Evolution of Planetary Systems"

1 Introduction

In our Solar System, there are several populations of small bodies, which differ both by their locations and by their physical properties. While most asteroids evolve in the main belt, a region located between the orbits of Mars and Jupiter, some of them originating from this region cross the orbits of the terrestrial planets (the so-called Near-Earth Objects or NEOs), while another population evolves on the same orbit as Jupiter on the L4 and L5 lagrangian points (the so-called Trojan asteroids). Then, another population of small bodies called Kuiper Belt Objects (or KBOs) evolves beyond the orbit of Neptune and is at the origin of the Jupiter-Family Comets (JFCs). Finally the Long Period Comets (LPCs) come temporarily in the Solar System from an external location called the Oort Cloud.

Small bodies of our Solar System are all affected by planetary gravitational perturbations. Thus, their orbits are more or less stable, depending on their locations. For instance, most NEOs are transported to Earth-crossing orbits from the main belt as a result of their injection into mean motion resonances with Jupiter, or secular ones with Saturn. These resonances increase their orbital eccentricity such that their perihelion distance becomes eventually shorter than 1 AU on only a few Myr timescale (e.g. [9], [5]). The population of JFCs is also transported from KBO orbits through resonant channels, and finally the LPCs are believed to come from the Oort cloud due to some stellar perturbations or galactic tides. Thus, these populations are all dynamically active.

In addition to these changes in their trajectories, small bodies of our Solar System can also undergo dramatic changes in their physical properties due to different mechanisms. Lightcurves obtained by ground-based observations, and images obtained from space missions, all show that these bodies can have very irregular shapes and heavily cratered surfaces, indicating a quite intense collisional activity. Moreover, spin rates give important clues about the composition and strength of these bodies. Then, the presence of binary objects, which represent about 15% of the main belt and NEO populations, indicates that some processes are efficient to form such systems.

So, what are the mechanisms that can modify the physical properties of a small body? We know at least three mechanisms which can be effective enough to change the shape or disrupt a small body, depending on its strength. The first most intuitive one is the collisional process. It is well known that populations of small bodies evolve collisionally. Witnesses of these collisional events are for instance the asteroid families in the main belt. About 20 asteroid families have been identified, and each corresponds to a group of small bodies who share the same orbital and spectral properties. From these characteristics, reproduced recently by numerical simulations (see, e.g. [30] and references therein), it is now established that an asteroid family is the outcome of the disruption of a large asteroid due to an impact with another small asteroid. As a consequence, a large asteroid is transformed into a group of smaller bodies,

and the shapes, sizes, spins and orbits of these objects depend on several parameters of the collision, one of them being the strength of the parent body. The second mechanism which can lead to a change of the physical properties of an object is the increase of its spin due to a thermal effect called the YORP effect ([43]). When a rotating body has an irregular shape, it can reemit the light received from the Sun in a different direction than the one from which it received it, and such difference in direction can lead to a change of its spin rate. Although acting on long timescales, such effect has recently been observed ([22]). When an acceleration occurs, depending on the strength and internal properties of the object, the spin can reach the threshold above which the shape of the body is not in equilibrium anymore, so that either the shape readjusts into another equilibrium or the body breaks up. The third mechanism which can produce similar effects is due to tidal encounters with a massive object (a planet). It is well known that below a certain limit distance, tidal forces can cause the deformation or the disruption of an object. This distance is known as the Roche limit for fluid bodies ([38], but as we will see, it can take different values and the bodies can take a wide range of shapes at this distance when solid materials (with and without cohesion) are considered.

The efficiency of all the mechanisms described above relies at least partially on the assumed strength of the small body on which these mechanisms act. This is why it is important that the definition of strength is clearly understood, and this paper addresses this problem. In Section 2, the definition of strength is given for different kinds of materials. Section 3 summarizes the most recent study on the spin limits of small bodies and what the observed spins tell us on the strength and internal structure of these objects. The latest results on the limit distances of small bodies to a planet as a function of their strength are then presented in Section 4. Several reviews have already been devoted to our current understanding of the collisional disruption of small bodies based on numerical simulations (see., e.g., [29], [30]), therefore this problem is briefly discussed in Section 5, concentrating only on the some important issues and open areas. Discussions, conclusions and perspectives are then given in Section 6.

2 The strength of materials

2.1 What do we mean by strength?

The behavior of a small solid body subjected to different forces is a wide area of research, and the results depend at least partially on the definition used for the strength of the material. In this section, we expose some important concepts which can help better understand the meaning of strength of a small body.

There is no doubt that the term "strength" is often used in imprecise ways. Given the implications of this concept in different areas of study, we believe

that it is important to present it in different places to ensure that a same language is spoken among researchers dealing with it. The description presented here is largely inspired from different works by Holsapple, and Holsapple and Michel ([15], [16] and [31]). Materials such as rocks, soils and ices, which are the main constituents of small bodies of our Solar System, are complex and characterized by several kinds of strength.

Generally, the concept of "strength" is a measure of an ability to withstand stress. But stress, as a tensor, can take on many different forms. One of the simplest is a uniaxial tension, for which one principal stress is positive and the two others are zero. The tensile strength, i.e. the value of this stress at which the specimen breaks, is often (mis)used to characterize material strength as a whole. Thus, while it is common to equate "zero tensile strength" to a fluid body, that is not correct. In fact, a body can both be solid and have no tensile strength. For instance, dry sand has no tensile strength. However, contrary to a fluid, dry sand and granular materials in general can withstand considerable shear stress when they are under pressure: that is why we can walk on dry sand but not on water. Here comes into play a second kind of strength: the shear strength which measures the ability to withstand pure shear. The shear strength in a granular material under confining pressure comes from the fact that the interlocking particles must move apart to slide over one another, and the confining pressure resists that. A third kind of strength, the compressive strength, governs the ability to withstand compressive uniaxial stress. Thus, in general, a material has tensile strength, shear strength at zero pressure (technically the "cohesion") and compressive strength. In geological materials such as soils and rocks, the failure stresses depend strongly on the confining pressure; as a result, these three strength values can be markedly different. Then, contrary to a common assumption, a cohesionless body is simply a solid body whose cohesion (shear strength at zero pressure) is null, but that does not mean it does not have any shear strength under confining pressure. For instance, there are strong evidence that probably most asteroids greater than a few kilometers in diameter are rubble piles or gravitational aggregates (see [36] for a definition of those terms). For such bodies, cohesion can be ignored but they should not be represented by a fluid. In their case, the confining pressure at the origin of the shear strength is played by their self-gravity. Hence, a body can be cohesionless but nevertheless solid.

2.2 Failure criteria of solid bodies

Once the strength of a material has been defined consistently, a failure law is required to determine imminent failure states of stress. Failure criteria for geological materials parallel the yield criteria for metals. Recall that the maximum stress at which a load can be applied without causing any permanent deformation defines the *elastic limit*. It is also called the *yield point*, for it marks the initiation of plastic or irreversible deformation.

There are two common yield criteria for metals: the Tresca criterion and the von Mises criterion. The Tresca criterion states that yield occurs when the maximum shear stress on any plane reaches a critical value. The von Mises criterion replaces the shear stress with the square root of the second invariant J_2 of the deviatoric stress tensor (non-diagonal components of the stress tensor), which depends on all shear stresses. A common assumption of these criteria is that the average stress (pressure), given in terms of principal stresses σ_i as $P = (\sigma_1 + \sigma_2 + \sigma_3)/3$, has no effect. Then, in a plane in principal stress space perpendicular to the pure pressure axis, the von Mises criterion is a circle, while the Tresca criterion is a hexagon (see, for example, [7] for a good discussion of various yield and failure criteria).

For geological materials, failure can also be described by two such criteria, but with an important addition: because the allowable shear depends on the confining pressure, the size of either of the circle or hexagon depends on the pressure or normal stress. The Mohr-Coulomb criterion (MC) assumes that the maximum shear stress on any plane (τ_{max}) depends linearly on the normal stress (σ_n) on the plane:

$$\tau_{max} = Y - \sigma_n \tan(\phi) \quad (1)$$

where the constant of proportionality is the tangent of the *angle of friction* ϕ , and the constant Y is called the *cohesion* (shear strength at zero pressure); both are material constants determined by experiments. This defines an envelope (limit curve) of maximum shear stress. Thus, compressive stress (negative) increases the allowable shear. In three-dimensional principal stress space, this criterion defines a hexagonal cylinder that increases linearly in size for increasing pressure ([7]). The MC criterion can be considered a Tresca criterion generalized to account for the normal stress effect.

Another criterion called Drucker-Prager (DP) is also common model for geological materials. The DP criterion can be considered a modification of the von Mises criterion, which now assumes that the allowable shear stress depends linearly on the confining pressure. The shear stress magnitude is measured by the square root of the second invariant J_2 of the deviator stress (see Eq. 3). Thus, the DP criterion is similar to models for linear friction and is defined by two constants: one characterizes the "cohesion" (shear strength at zero pressure), and the second characterizes the dependence on the confining pressure and is related to the angle of friction. Those two constants determine the tensile and compressive strengths. When the cohesion is zero, so is the tensile strength, but not the compressive strength. Physically, the pressure dependence is, as already explained, the consequence of the interlocking of the granular particles and not the friction of the surfaces of the particles. In fact, a closely packed mass of uniform rigid *frictionless* spherical particles has an angle of friction about 23° . So the term angle of friction is somewhat a misnomer and angle of *interlocking* would be more correct. However, we will keep using the usual name angle of friction. Figure 1 gives a representation of the DP model. Using the three principal stresses σ_1 , σ_2 , σ_3 (positive in

tension) of a general three-dimensional stress state, the pressure (positive in tension) is given as:

$$P = \frac{1}{3}(\sigma_1 + \sigma_2 + \sigma_3) \quad (2)$$

and the square root of the second invariant of the deviator stress is:

$$\sqrt{J_2} = \frac{1}{\sqrt{6}}\sqrt{[(\sigma_1 - \sigma_2)^2 + (\sigma_2 - \sigma_3)^2 + (\sigma_3 - \sigma_1)^2]} \quad (3)$$

Then, the DP failure criterion is generally given as:

$$\sqrt{J_2} \leq k - 3sP \quad (4)$$

which is illustrated as a straight line with slope $3s$ and intercept k on Fig. 1. Clearly negative pressure (compression) increases the allowable $\sqrt{J_2}$ when s is positive.

For the special case of a pure shear stress only, $\sqrt{J_2}$ is just that shear stress and the pressure P is zero. On Fig. 1, the uniaxial tension strength σ_T has $\sqrt{J_2} = 3^{-1/2}\sigma_T$ and $P = \sigma_T/3$. The uniaxial compression strength σ_C has $\sqrt{J_2} = -3^{-1/2}\sigma_C$ and $P = \sigma_C/3$.

The DP criterion can be made to match the MC one in all combinations of pressure plus uniaxial compression if the parameters s and k are related to the cohesion and the angle of friction ϕ used in the MC model. In particular, the slope s is related to the angle of friction ϕ of the MC model by:

$$s = \frac{2 \sin \phi}{\sqrt{3}(3 - \sin \phi)}. \quad (5)$$

The intercept k of the DP model is also the shear stress τ for failure in pure shear. Technically the term "cohesion" means this intercept value of shear stress at zero pressure. When the cohesion is zero, so is the tensile strength, and vice versa; both cases would have the envelope starting at the origin on Fig. 1. For instance, an appropriate failure criterion for rubble piles is a criterion for which those two measures are zero, while the plot shows the more general case where they are non-zero.

The tensile stress σ_T for failure is located at the intersection of the tensile line shown on Fig. 1 sloping to the left with the straight line representing the criterion. Its value is given by:

$$\sigma_T = \frac{\sqrt{3}}{\sqrt{3}s + 1}k. \quad (6)$$

Similarly, the compressive failure occurs when the compression line intercepts the failure line, and the resulting compressive stress is given by:

$$\sigma_P = \frac{\sqrt{3}}{\sqrt{3}s + 1}k. \quad (7)$$

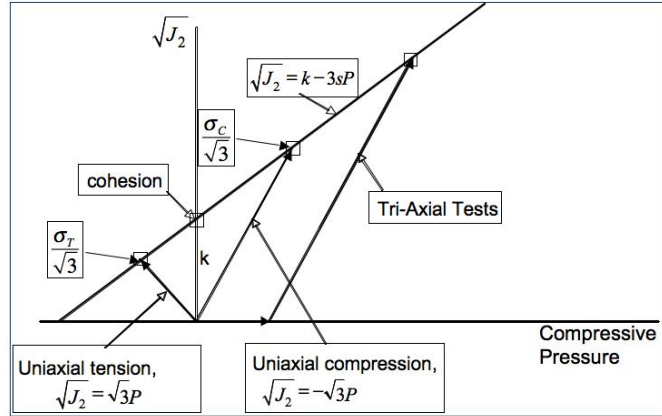


Fig. 1. The Drucker-Prager failure criterion. The abscissa is positive in compression. The four small squares indicate the failure condition in, respectively from the left: tension, shear, compression and a confined compression or tri-axial test. The intercept at zero pressure at the value k is called the cohesion and the slope of the line passing through k is $3s$. From [16] and [31].

Hence, the ratio of compressive strength to tensile strength is given by:

$$\frac{\sigma_C}{\sigma_T} = \frac{\sqrt{3}s + 1}{\sqrt{3}s - 1} \quad (8)$$

which defines the slope of the DP criterion, i.e. the friction coefficient s .

To give an order of idea of the difference between those strengths, a common friction angle for rocks is 45° , so that $s = 0.356$, and the ratio of compressive strength to tensile strength is $-4.22 : 1$. In this case, from Eq. (6), the shear stress for failure k would be 0.93 of σ_T , i.e. the shear and tensile strengths are roughly equal.

This envelope is usually determined experimentally by a test known as a "confined compression" or a "tri-axial" test. In such a test, a uniform confining pressure is applied to a specimen in all directions, and the axial stress is increased in compression until failure occurs when the envelope is reached. This path is illustrated on Fig. 1.

Finally, from a practical point of view, the two criteria (MC and DP) can offer different advantages. The MC model defines a maximum shear stress

directly, which is determined by the difference of the maximum and minimum principal stresses. As a consequence, to use this criterion in algebraic manipulations involving general stress states, one must first determine the principal stresses, then which is the largest and which is the smallest. The result is a difference in the algebra of the results in six different regimes, where the three principal stress components take on different orderings. An example of the six possible cases of the ordering of the stress magnitudes is given in Fig. 4 of [12]. Moreover, there are "corners" in the curves shown where the ordering of the principal stresses changes. In contrast, the DP criterion has a single algebraic relation for all stress states. Thus, although the algebraic form of that relation is more complicated than the MC criterion, there is no need to consider the six different possibilities of the ordering of the stress magnitudes. The algebraic complexity of the DP model is of little consequence when an algebraic manipulation program such as *Mathematica* is used. For instance, Holsapple and Michel used the DP failure criterion to characterize the tidal disruption limit distance of a cohesionless ellipsoid to a planet, noting that the differences between the two models are small (see [15] and Sect. 4).

2.3 Strength dependence on object's size and loading rate

It is generally believed that the effective static cohesive and tensile strengths decrease with increasing body size. The origin of this assumption comes from indications that a distribution of incipient flaws is present within the volume of a solid body. Because larger bodies are more likely to contain larger natural flaws than smaller bodies, the strength is expected to decrease with the body's size. Thus, the use of a strength measure that decreases with size is now a common feature of the studies of disruption of small bodies by impacts (see, e.g. [13], [30]) and has even been demonstrated experimentally ([19]).

A common model for a distribution of incipient flaws in a solid body is a power-law Weibull distribution ([45]). Such a distribution is used in numerical simulations of catastrophic disruption of solid bodies (see Sect. 5) to generate the initial flaws in the bodies involved. A two-parameter Weibull distribution is usually assumed to describe the network of incipient flaws in any material, expressed as:

$$N(\varepsilon) = k\varepsilon^m \quad (9)$$

where ε is the strain and N is the number density of flaws that activate (i.e. start their propagation) at or below this value of strain. The Weibull parameters m and k are material constants which have been measured for a number of geological and industrial materials, although data are quite scarce for some important rocks (see [24]). In particular the parameter k varies widely between various rock types and the exponent m ranges typically between 6 and 12, but can have a wider range of values. Recently it was measured for the first time for the same basalt material as the one used in some impact experiments, and its value was found to be around 17 in static loadings ([33]).

From the Weibull distribution, it is easily shown that the most probable static strength S of a specimen of volume V (diameter D) decreases with increasing size as:

$$S \propto V^{-1/m} \propto D^{-3/m}. \quad (10)$$

As explained above, such a decrease in strength is simply because larger specimens are more likely to have larger cracks.

The values of the Weibull parameters represent important material properties. Large values of m describe homogeneous rocks with uniform fracture threshold, while small values apply to rocks with widely varying flaw activation thresholds. The existence of incipient flaws within any rock is understood to originate from its cooling history and from crystal lattice imperfections. Due to the initial presence of these flaws, when a finite strain rate $\dot{\epsilon}$ is applied, a stress increase occurs in time, which is compensated by the propagation of active flaws causing a stress release. Thus a competition takes place between the stress increase due to loading and the stress release due to flaw activation and propagation, until a temporary equilibrium is reached at the time of peak stress. Then, the stress decreases to zero as active flaws propagate rapidly through the rock.

From these explanations, it is obvious that the crack growth velocity c_g is an important parameter since it governs the stress release due to an active flaw. Experiments indicate that it relates to the speed c_l of longitudinal waves in a rock by $c_g \approx 0.4c_l$, and this is usually the value used in numerical simulations of fragmentation. Since cracks propagate at this fixed velocity, under moderate conditions, the weakest flaws (those which activate at lower values of ϵ) suffice to accommodate the growing stresses. Therefore, the peak stress at failure is low and fragments are relatively large (see, e.g., Fig. 1 in [30]). Conversely, more resistant flaws have time to activate at high strain rates. In this case, the peak failure stress is high and fragments are small. This process depends strongly on the assumed value of the crack growth velocity c_g . In particular, fragment sizes scale with c_g . For instance, a higher velocity would enhance the efficiency at which a crack relieves stress, since stress release is proportional to crack length cubed. As a consequence, fewer flaws would be required to relieve a given increase in stress.

Thus, the concept of material strength reaches another level of complexity as it can also depend on the dynamical context. From the explanations above, one may conclude that defining the material strength as *the stress at which sudden failure occurs* is not rigorously adequate. Material strength could rather be defined as the stress at which the first flaw begins to fail, thereby initiating an inelastic behavior characterized by irreversible deformation. But in practice, the adopted definition is the peak stress which the rock undergoes prior to failure. It is then not a material constant, since as explained above, the peak stress is a function of the loading history of the rock. This is the reason why a distinction is made between static strength and dynamic strength on the basis of the loading rate. For extremely small loading rates,

elastic stresses increase in equilibrium until the onset of catastrophic failure. This occurs at loading rates that are typically smaller than $\approx 10^{-6}$ strains per second. Static tensile strength decreases with increasing size of the rock due to the greater probability of finding a weaker (larger) flaw. At high enough loading rates, stresses can continue to build while catastrophic rupture has begun. In this case, it is more appropriate to speak of dynamic failure. For most rocks, dynamic strain rates are of the order of 1 s^{-1} and decrease with increasing rock size. Therefore, the peak stress that the rock suffers prior to failure is rigorously called the material's dynamic strength at that strain rate. This dynamic strength increases with strain rate and is always greater than the static strength.

All hypervelocity impacts into small targets are in the dynamic regime, but some impacts on large bodies can still be in a regime close to the static one. In this case, part of the event, close to the impact point, can be dynamic, but some important aspects can also be understood in terms of quasi-static failure. Therefore, in all studies that are described in the following sections, apart from the problem of catastrophic disruption, the tensile strength will generally be the static one.

3 Rotation rates and implications on the strength of small bodies

The spin rates of small bodies of the Solar System give an important clue about the composition and strength of those bodies. Indeed, the greatest spin that a body can take without being deformed or disrupted depends directly on those properties. For instance, a simple analysis based on the property of zero tensile stresses at the body's poles ([11]) led to the conclusion that an object whose assumed typical mass density is 2.5 g/cm^3 has a period limit of 2.1 h. This value is smaller than the measured rotation period of all large asteroids. Thus, it was suggested that most asteroids must be gravitational aggregates or rubble piles with no tensile strength. This value was later revised ([12], [14]) by a complete stress analysis of spinning, self-gravitating, ellipsoidal bodies using the MC failure criterion for cohesionless solid bodies (see Sect. 2.2). From this analysis, it was concluded that the spin limits are not determined by tensile failure, but by shear failure. Consequently, it was found that the spin limits depend on the angle of friction (see Sect. 2.2) of the material of the body. A typical minimum period was found to be about 2.6 h, which is higher than the previous estimate ([11]), but still smaller than the rotation period of large asteroids. Numerical experiments of spinning rubble piles (modeled as hard spheres maintained together by gravity) found that such rubble-piles behave in a manner consistent with those last theoretical expectations ([37]).

It was thus tempting to conclude on this basis that most asteroids are rubble piles, because none of them was found to rotate faster than the limit above which a rubble pile would break, in principle. However, recent data

for small asteroids indicated that some of them rotate at a rate which is much greater than those previous limits, which suggests that they have some cohesive and tensile strength. This raised the question whether the spin limits observed for large asteroids really rule out that their material is strengthless.

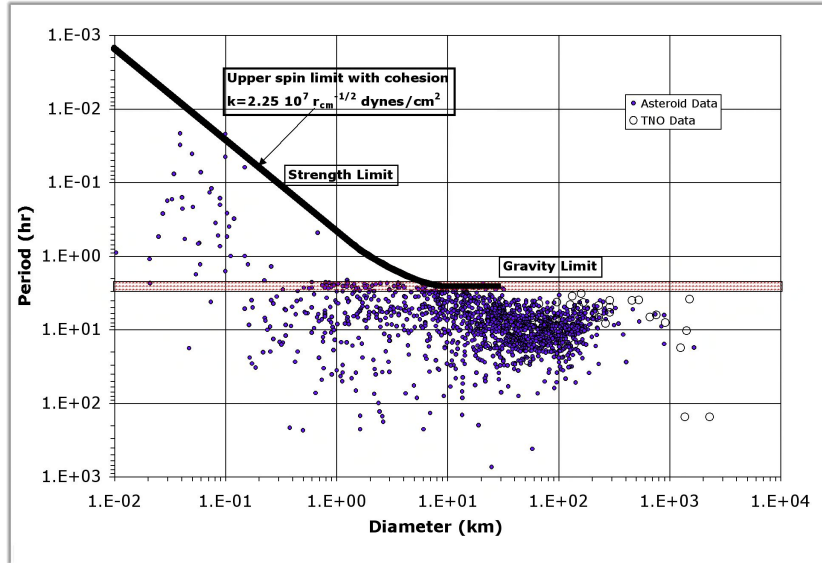


Fig. 2. Spin limits and data for small Solar System bodies. The dark sloped line assumes a size dependent strength; it becomes asymptotic to the horizontal red band for materials without cohesion. On the left, the spin limit for cohesive bodies is determined by the cohesive/tensile strength and defines a strength regime. The horizontal asymptote on the right characterizes a gravity regime where tensile/cohesive strength is of no consequence. Gravity regime values do depend on shape and angle of friction, so average values have been assumed to represent them on the plot. The data in the upper left triangular region are the fast spinning near-Earth asteroids. The triangular points for the large diameter bodies on the right are trans-Neptunian objects (from [16] and [18]).

These questions have been addressed in a recent study ([16]), and this section summarizes its principle and main results. It is an extension of previous studies ([12], [14]) and considers spinning bodies with cohesive (and therefore tensile) strength. The fundamental approach consisted of calculating the internal stress state in an ellipsoidal spinning body as a function of size, shape and spin of the body, and comparing the stress state with the limit failure state (provided by the DP model; see Sect. 2.2) to determine the spin limits at which the failure occurs. It must be noted that rather than solving for the stress state by assuming linear elasticity from some actual prior history of the material, the limit states are solved in the spirit of limit analyses of

plasticity theories. Those limit states correspond to the situation when the body has reached a final state at which collapse is imminent, and give the final and greatest loadings for failure. The great advantage of this approach is that the prior history of the material is not a factor, and the analyses give a limiting loading state with a greater spin than any found from first failure using a linear elastic approach. This is important because small bodies of our Solar System are formed by complex processes and undergo disruptions, reacumulations, heating, cratering events, tidal forces and so on. Those processes inevitably introduce residual stresses that cannot be known, so the assumption of linear elastic behavior from a virgin stress-free state is not reasonable given the history of these bodies. There exist several explicit examples (see [15]) that illustrate the important differences between stress analyses using elasticity theory, and those using the limit state approach. This limit state approach will also be used to determine the tidal disruption limit distances of solid bodies ([15], [18], [31]; see Sect. 4).

A significant complexity is added once the cohesive terms are included in the strength measure. Indeed, for a cohesionless failure criterion, it was found ([14]) that the limit states had simultaneous failure at all points in the body and the algebra to find that state was rather simple. When the material has cohesion, failure is rather attained only at certain points and planes within the body, and the algebra that determines the stress state with certain failure locations seems insurmountable (even for a symbolic program such as *Mathematica*). Therefore, the approach chosen by Holsapple in his study was to construct the volume-averaged stresses and to use those stresses to compare to the failure criterion ([16]). In other words, spin states are determined which, on average, cause stresses to equal the failure threshold (see Sec. 2.2). It is clear that for a body having a certain degree of cohesion, more or less critical stress states than the average may exist at some locations within the body, so in reality failure may occur at a lower spin than that found with this approach. But in the particular case of a cohesionless material, failure occurs at all locations in the body at the limit spin. Therefore in this case, both the average and the exact methods give identical results. In other words, in the gravity regime (in which self-gravity dominates over strength, so that cohesion can be ignored) the results are exact, while in the strength regime (in which self-gravity is negligible) they are only approximate.

Once the average stresses have been expressed ([16]), they can be inserted into the DP criterion (Eq. (4)) to find the combinations of spin and shape that satisfy this criterion. Then for a given shape, represented by the aspect ratios of an ellipsoid, the spin at a given limit state can be found. Defining a scaled spin as:

$$\Omega^2 = \frac{\omega^2}{\pi\rho G}, \quad (11)$$

where ω is the actual spin, ρ is the bulk density and G is the gravitational constant, the results can be put into the form of relations for the scaled spin at failure states as functions of the cohesion, the angle of friction ϕ (see Sect.

2.2), the average body radius $\bar{r} = (abc)^{1/3}$ (where a , b and c are the semi-axes of the ellipsoid representing the object with $a > b > c$) and the two aspect ratios $\alpha = c/a$ and $\beta = b/a$:

$$\Omega = F(k, \phi, \bar{r}, \alpha, \beta). \quad (12)$$

The spin limits are indicated on Fig. 2. Both constant strength and decreasing strength with body size have been considered. For the size-dependent strength (see Sect. 2.3), the value assumed for the Weibull parameter m (Eq. (9)) is $m = 6$, which seems to fit many data for crack distributions in samples from micron to kilometer sizes ([19]). From Eq. (10), for $m = 6$, the strength of a body decreases with the body's diameter to the power of $-1/2$. Therefore, the strength (cohesion) expresses as:

$$k = \kappa \bar{r}^{-1/2} \quad (13)$$

where the strength coefficient κ is the strength of an object of 1 cm in radius (here k is used for the cohesion and should not be confused with the Weibull parameter having the same name). The spin limits represented on Fig. 2 have been estimated assuming $\kappa = 2.25 \times 10^7$ dynes/cm^{3/2}, which is one order of magnitude below the measurements of the tensile strength of Georgia Keystone granite specimens ([19]). The sloped line corresponding to this size-variable strength (Fig. 2) gives an extremely good upper envelope for the current data over the entire range of small body sizes. Measured strengths are still scarce, so it is not necessarily surprising that the best fit is provided by the line corresponding to a strength value smaller than the measured one.

Note that these estimates of spin limits by Holsapple ([16]) assume that the bodies have ideal ellipsoidal shapes (with aspect ratios of 0.7 and prolate for the representation on the figure) and a fixed friction angle. The reality is obviously more complex, which may explain that the observed spin limits are smaller than the ones assuming the measured tensile strength. In particular, small bodies do not have ideal shapes, their actual friction angle is not known, they may have weaker materials and other non-ideal properties. Moreover, determinations of the observed body's sizes and shapes contain their own error bars which may shift the points on Figure 2 toward higher or lower values. Note finally that the magnitude of the dependence of the estimated spin limit on shape and friction angle is well within a factor two, except in extreme cases. Also, the average method used to make those estimates gives an upper bound to the limit spin in the strength regime.

Thus, a detailed investigation of the spin limits as a function of the mentioned parameters, including strength, has been performed recently by Holsapple ([16]) and the conclusion of this investigation is rich in implications. In particular, it is found that the presence of tensile and cohesive strength for a large body (> 10 km in diameter) makes no difference in its spin limit. Therefore, the observed spin limit (also called the spin barrier) for large bodies cannot be interpreted as evidence of a zero-strength (cohesive/tensile) rubble

pile structure. It is the gravity that limits the spin in those cases, even if they have some cohesion. So, large asteroids may be rubble piles, but not on the pure basis of the so-called spin barrier (however, other evidence may point to a rubble pile structure). On the other hand, the strength that allows the higher spins of the smaller and fast spinning km-sized bodies is only of the order of 10-100 kPa, which is very small compared to the strength of small terrestrial rocks. So, these small asteroids do not have to be very strong to be able to rotate so fast. They could be some kind of rubble piles that have accumulated slight bondings between constituents.

As a conclusion, the spin data of small bodies can give us some indications on the internal structure of these bodies. However, based on the current observed spins and our current understanding on the strength of large bodies, they are not sufficient to indicate whether these bodies are rubble-piles or monolithics. If some small asteroids were found to spin above the theoretical limits provided by the described approach ([16]), then this would be a first indication of the potential existence of strong (monolithic) rocky bodies in the Solar System.

4 Tidal disruption of small bodies

When a small body has a close encounter with a planet, depending on the approach distance, it can be subjected to tidal forces that may change its shape or even disrupt it. Such mechanism was at the origin of the observed disruption of Comet Shoemaker-Levy 9, which was fragmented into 21 pieces during a first passage close to Jupiter, and which collided with the giant planet during its next passage in 1994. Tidal disruption has often been proposed as a formation mechanism for binary asteroids, which represent 15% of the Near-Earth Object population, and as an explanation of crater chains and doublet craters on planetary surfaces. The strength of a small body is an important parameter in the determination of its limit distance to a planet for tidal disruption (or shape readjustment).

The investigation of the limit distance for tidal disruption started in the 19th century, using a fluid to represent the small body. This led to the concept of the Roche limit ([38]), which is still often used nowadays. A great numbers of studies followed until now, which accounted for important parameters in different manners from one study to the other. The last theoretical studies on this problem provided a continuum theory which allows the determination of this limit distance for cohesionless bodies, and a lower bound of this distance for small bodies with cohesion ([15], [31], [18]). We summarize here the theory and results provided by these studies, and the reader interested in other previous studies on these problems can refer to these last publications in which a history of previous works and their differences are well exposed.

Although the Roche limit ([38]) for tidal disruption of orbiting satellites assumes a fluid body, a length to diameter of exactly 2.07 : 1, and a particular

orientation of the body, it is often used in studies of Solar System satellites and small asteroids or comets encountering a planet. Clearly, these bodies are neither fluid, nor generally are that elongated, so more appropriate theories are needed and have been developed since this first work. Recently, exact analytical results for the distortion and disruption limits of solid spinning ellipsoid bodies subjected to tidal forces, using the DP model with zero cohesion (see Sect. 2.2) have been presented ([15]). The study used the same approach as the one exposed in Sect. 3 to study the spin limits for solid ellipsoidal bodies. It was followed by a study along the same lines, in which the cohesion of the small bodies was now considered, which, due to the added complexity, could not provide exact but only approximate results ([18]), for the same reasons as the ones already exposed in the case of spin limits (see Sect. 3). Thus, a static theory was developed that predicts conditions for breakup, the nature of the deformation at the limit state, but it does not track the dynamics of the body as it comes apart. At the end of the section, we will briefly expose results from dynamical investigations.

In the case of cohesionless bodies, as already indicated in previous sections, the strength is essentially characterized by a single parameter associated with an angle of friction ranging from 0° to 90° . The case with a null angle of friction has no shear strength whatsoever, so it corresponds to the case of a fluid or a gas (and the limit distance corresponds to the Roche limit). The case of 90° represents a material that cannot fail in shear, but still has zero tensile strength. Typical dry soils have angles of friction of 30° - 40° . As most satellites are spin-locked with the planet around which they evolve, both the spin-locked case and the zero spin case, a possible case for passing stray body, have been considered to characterize the limit distance.

The equilibrium problem of an ellipsoid body has been described by Holsapple ([12]). Three stress equilibrium equations must be satisfied by the stresses σ_{ij} in any body in static equilibrium with body forces b_i , which are given as (using repeated index summation convention):

$$\frac{\partial}{\partial x_j} \sigma_{ij} + \rho b_i = 0 \quad (14)$$

where ρ is the bulk density of the body. An (x, y, z) coordinate system aligned with the ordered principal axes of the ellipsoid is used. In the problems here, the body forces arise from mutual gravitational forces, centrifugal forces, and/or tidal forces; they all have the simple linear forms $b_x = k_x x$, $b_y = k_y y$, $b_z = k_z z$. The full expressions of k_x , k_y and k_z are explicitly presented by Holsapple and Michel ([15]). Then, for the limit states sought, the stresses must satisfy the DP failure criterion (see Sect. 2.2) at all points x , y and z . Also, the surface tensions are zero on the surface points of the ellipsoidal body surface defined by: $\frac{x^2}{a^2} + \frac{y^2}{b^2} + \frac{z^2}{c^2} - 1 = 0$. This problem has been solved ([12]), showing that the distribution of stresses in that limit state just at uniform global failure has the simple form:

$$\begin{aligned}
\sigma_x &= -\rho k_x a^2 \left[1 - \left(\frac{x}{a}\right)^2 - \left(\frac{y}{b}\right)^2 - \left(\frac{z}{c}\right)^2 \right], \\
\sigma_y &= -\rho k_y b^2 \left[1 - \left(\frac{x}{a}\right)^2 - \left(\frac{y}{b}\right)^2 - \left(\frac{z}{c}\right)^2 \right], \\
\sigma_z &= -\rho k_z c^2 \left[1 - \left(\frac{x}{a}\right)^2 - \left(\frac{y}{b}\right)^2 - \left(\frac{z}{c}\right)^2 \right],
\end{aligned} \tag{15}$$

and the shear stresses in this coordinate system are all zero. The body force constants k_x , k_y , k_z depend on the body forces, so those forces must be such that the DP failure criterion is not violated. That condition determines the limit states. Putting the expressions of these components into the DP criterion (Eq. (4)), one can see that the common functional dependence $1 - \left(\frac{x}{a}\right)^2 - \left(\frac{y}{b}\right)^2 - \left(\frac{z}{c}\right)^2$ will cancel out of the Eq. (15). That is because the limit stress state has simultaneous failure at all points. Thus, we can omit that functional dependence and focus on finding the combinations of the leading multipliers of the three terms of Eq. (15) that satisfy the failure criterion. We define the dimensionless distance by:

$$\delta = \left(\frac{\rho}{\rho_p}\right)^{1/3} \frac{d}{R} \tag{16}$$

where ρ_p is the bulk density of the primary (the planet). Then, as detailed by Holsapple and Michel ([15]), failure will occur when:

$$\frac{1}{6} [(c_x - c_y)^2 + (c_y - c_z)^2 + (c_z - c_x)^2] = s^2 [c_x + c_y + c_z]^2 \tag{17}$$

where, for arbitrary spin and when the long axis points towards the Earth:

$$\begin{aligned}
c_x &= \left(-A_x + \frac{1}{2}\Omega^2 + \frac{4}{3}\delta^{-3}\right), \\
c_y &= \beta^2 \left(-A_y + \frac{1}{2}\Omega^2 - \frac{2}{3}\delta^{-3}\right), \\
c_z &= \alpha^2 \left(-A_z - \frac{2}{3}\delta^{-3}\right)
\end{aligned} \tag{18}$$

and A_x , A_y and A_z are the components of the self-gravitational potential of a homogeneous ellipsoidal body of uniform mass density ρ in the body coordinate system expressed as: $U = \pi\rho G(A_0 + A_x x^2 + A_y y^2 + A_z z^2)$ (e.g. [6]). Ω is the scaled spin already expressed in Sect. 3. A similar form when the long axis points along the trajectory at its closest approach can be obtained ([15]). The criterion expressed in these forms can then be used to solve for the dimensionless distances δ at the failure condition as a function of the aspect ratios α and β (which determine the A_x , A_y and A_z), the mass ratio p of the secondary to the primary, and for any value of the constant s related to the angle of friction. The solution always has the dimensionless form:

$$\delta = \frac{d}{R} \left(\frac{\rho}{\rho_p} \right)^{1/3} = F[\alpha, \beta, p, \phi, \Omega] \quad (19)$$

so that the bulk density ratio only occurs with this cube root. Note that in the spin-locked case, the spin is given by:

$$\omega = \frac{G(M + m)}{d^3} \quad (20)$$

where M and m are the masses of the primary and secondary, respectively. The number of independent variables is then reduced by one when the scaled spin is zero or the spin-locked value, and by another one when $p = 0$, i.e. when the mass of the secondary is negligible compared to that of the primary, which is the case for an asteroid flying by a planet or a small satellite of a giant planet.

Note that this limit distance to the primary corresponds to the distance below which a secondary cannot exist with its assumed shape, because the failure criterion would be violated. However, it does not mean that below this distance, the secondary would disrupt. A flow rule is required to indicate the nature of any readjustment (or disruption). Then, if those changes lead to a new configuration that is within failure at the given distance, a shape change is indicated. Otherwise, if the new shape still violates the failure criterion, a global disruption is indicated. Such analysis has been done by Holsapple and Michel ([15]) but goes beyond the scope of this review.

The results provided by this static theory show that a spin-locked spherical body can approach a planet as close as $d/R = 1.23168(\rho_p/\rho)^{1/3}$ if its angle of friction is 90° , and the orbit distance decreases smoothly as the angle of friction increases. For a generic rock value, say $\phi = 30^\circ$, the closest orbit for a spherical satellite is about $d/R = 1.5(\rho_p/\rho)^{1/3}$. The fluid case with zero angle of friction has a distance of infinity, as there is no solution for a spherical body in this case. Other general ellipsoid shapes have then been fully investigated, and it was found that for each combinations of aspect ratios α and β , there is a range of permissible orbital distances for any angle of friction $\phi > 0^\circ$. For instance, a prolate body of negligible mass with aspect ratios of 0.8 and $\phi = 20^\circ$ can orbit as close as $d/R = 1.78261(\rho_p/\rho)^{1/3}$, center to center, and if $\phi = 40^\circ$, it can orbit as close as $d/R = 1.15141(\rho_p/\rho)^{1/3}$. Then, an elongated prolate body with $\alpha = 0.4$ and $\phi = 40^\circ$ can orbit as close as $d/R = 1.92929(\rho_p/\rho)^{1/3}$. Figure 3 illustrates the same application to a stray body with zero spin, $p = 0$ and $\alpha = 0.8$.

Thus, all of these are noticeably closer than the fluid Roche limit of $d/R = 2.455(\rho_p/\rho)^{1/3}$, and for a solid, even cohesionless, the shapes are not limited to fluid shapes. This is why it is important to make no confusion between a fluid and a cohesionless bodies. This is particularly important in the context of the study of satellites of giant planets. In fact, many planetary satellites are inside their Roche limit, and do not have the aspect ratios required for a fluid at this limit (see e.g. Table 1 in [15]). The same holds true for stray

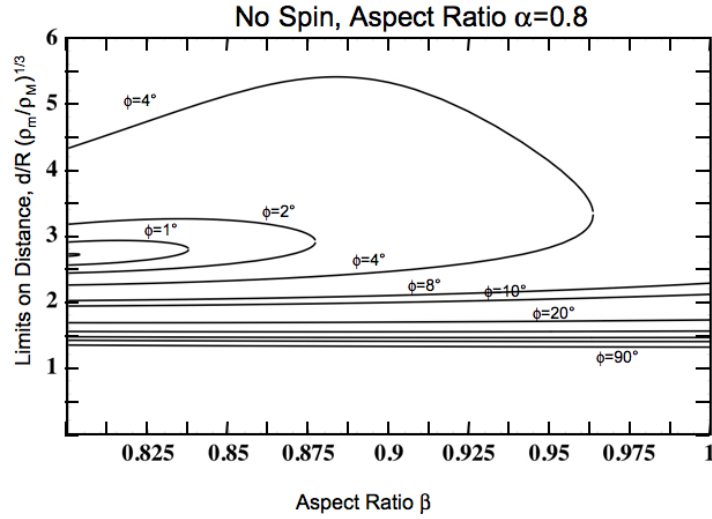


Fig. 3. Limits on the possible distances for a stray body with no spin and for various aspect ratios α and β , and different angles of friction Φ . Note that for small angles of friction, the region of permissible distances is a closed curve. This means that the body cannot approach too close, because tidal forces would be too strong, nor range too far as some tidal forces are still necessary for its equilibrium. The limit case of such behavior is the Roche fluid case, for which there is a single point at the center of the closed curves, near the prolate bodies on the left. For typical angles of friction (20° to 40°), there is no large variation with the aspect ratios. As in the spin-locked situation, the minimum distances for cohesionless stray bodies are all well below the Roche limit, and a much wider range of aspect ratios can exist.

(zero-spin) cohesionless bodies (the case of a fluid body in this configuration is called the Jean's problem, [21]).

The difference with a fluid body is even more striking when cohesion is added to the strength of a small body. This has been investigated recently by Holsapple and Michel ([18]) who extended their previous analysis of limit distances of cohesionless ellipsoids to the limit distances of ellipsoids with cohesion. Recall that when the cohesion term k is zero in the DP criterion (Eq. (4)), the general form of the stresses satisfying the equilibrium condition, the boundary values and the failure criterion at all points in the body can be found exactly in closed form with a quadratic dependence on the coordinates. Conversely, when the cohesion is not zero, there is no solution to this general equilibrium problem with simultaneous failure at all locations. Therefore, an exact answer cannot be determined, but an approximate solution can be found by averaging the stresses across the body, as explained in Sect. 3 for the spin

limits. The difference here with the spin limit study is that the tidal terms are added. It has been proven that the loads for which the average stresses are at failure are equal to or greater than the actual limit loads ([17]). thus, using average stresses to look for failure gives an upper bound on actual limit loads. In other words, the analysis provides a lower bound to the closest approach for collapse. But recall again that in the special cases with zero cohesion the results are exact. In fact, a study along the same lines devoted to tidal encounters of granular bodies has been done by Sharma et al. using the volume average approach and, although the calculations of limit distances were not investigated with the same level of details, it was consistent with the results above using the closed form for the stresses ([39]).

The limit distance for a small cohesive body can be expressed in terms of 7 non-dimensional parameters (one dependent, six independent variables), leading for each orientation of the body to the reduced form:

$$\delta = \frac{d}{R} \left(\frac{\rho}{\rho_p} \right)^{1/3} = G[\alpha, \beta, p, \Omega, \phi, \frac{k}{\rho^2 Gr^2}] \quad (21)$$

using the previously defined aspect ratios α , β , mass ratio p , and a scaled cohesion term $k^* = k/(\rho^2 Gr^2)$, where r is the body's average radius. This scaled term corresponds to the ratio of the cohesive strength to a gravity pressure. For any given value of these six parameters, numerical results can then easily be obtained, using appropriate programs (see [18] for significant examples and illustrations of important dependencies). In this analysis, the cohesion is also assumed to decrease with the body's size, and the same size dependency as in Sect. 3 is used.

For bodies larger than a few km in diameter, the limit distance is the one provided by the theory for cohesionless bodies, as the cohesion is so small that gravity is dominant (due to the decrease of cohesion with size). Thus, the new approach in which cohesion is included is only relevant for those bodies whose size is below a few kilometers. For them, the limit distance becomes much closer to the primary, and depending on the values of the six parameters (or on the density ratio) the distance can even be smaller than the primary's radius, which means that these small bodies cannot be disrupted by tidal forces. An interesting application relates to planetary satellites, and a preliminary analysis showed that some of them must have non zero friction angles or cohesion to evolve at the observed distance from their primary (see [18]). Thus, the approach developed to determine limit distances can provide some indirect indications on the possible internal structure of real objects, which is a very interesting aspect. Also, it can tell us whether some shape readjustment or disruption will occur during the close approach with the Earth of a real asteroid. For instance, if we assume that the asteroid Apophis (2004 MN4) is a cohesionless body, then the static theory developed by Holsapple and Michel indicates that its close approach with the Earth at 5.6 Earth's radii in 2029 will correspond to its tidal limit distance only if its bulk density

is smaller than 0.25 g/cm^3 or unless it is highly elongated, or its angle of friction is less than about 5° ([15], [31]).

Thus, according to these recent studies, both cohesionless bodies and cohesive ones with expected properties of geological solids can exist in arbitrary ellipsoidal shapes and much closer to a primary than a fluid body. The main limitation of these studies is that they are not based on a dynamic approach but a static one, which is used to determine the onset of disruption or shape readjustment. Actually, in case of readjustment, the angular moment of inertia would change, so the spin would change. Then the new state would not be in the spin-locked or zero spin configuration as supposed here. The effects of tidal torques on the asteroid's spin have been investigated in details ([40], [41]), and a complete analysis should incorporate these results, thereby accounting for the change in the limit distance as the small body's spin rate changes during a fly-by. Such analysis will have to be performed in the future.

Also, when a small body goes through the limit distance, the resulting motions are affected by how the body changes its shape or breaks up, and by the resulting dynamics. That is a much more complicated problem, which is left for future studies. Some semi-analytical studies have been recently done to address this problem ([39], but numerical simulations are probably the best tools. In a pioneering numerical study ([34]), the break-up of bodies encountering a planet was considered. Small bodies were modeled as granular aggregates comprised of 247 smooth spheres that interacted with each other only through inelastic collisions and were held together by gravity. Numerical simulations were then used to determine the motion of individual spheres. Various parameters, such as the initial angular velocity vector and encounter variables, were changed to explore the consequences of different close approach configurations. But this study was limited by the low resolution (number of smooth spheres) constrained by the computer performances and numerical codes at that time. More recently, numerical simulations of tidal disruption of rubble piles at higher resolutions using a sophisticated N-body code named *pkdgrav* have been performed ([44]) in order to determine whether tidal disruptions can explain the presence of 15% of binaries in the NEO population. The results show that tidal encounters with a planet (Earth) can form binaries. However, when a small body experiences a tidal encounter, it is likely to experience another such encounter in its close future, so that the binary which is first formed is often eventually disrupted by the next encounter. Thus, although tidal encounters are efficient to form temporary binaries, they cannot be at the origin of the high fraction of binaries observed in the NEO population. Some other potential mechanisms must be found and investigated. Also, these simulations only addressed the problem of tidal approaches of cohesionless bodies, and they will be extended to the case of cohesive bodies in a close future. In principle, the limit distances should be similar to the ones provided by the static approach (for some values of the angle of friction and cohesion), but a dynamical approach will also allow the determination of the behavior of the small body and its separate pieces once it breaks up. The gravitational

To be published in:
 "Small Bodies in Planetary Systems".
 (Mann, Nakamura, Mukai eds.)

Submitted to Lecture Notes in Physics series by Springer
 Funded by the 21st Century COE Program
 "Origin and Evolution of Planetary Systems"

evolution of fragments from a disrupted body has already been studied but only in the specific case of the collisional disruption of a small body. This is the last mechanism of disruption which is briefly summarized in the following section.

5 Collisional disruption of small bodies

In this section, we just summarize the most important concepts and issues concerning the catastrophic disruption of an asteroid due to a collision. The reader interested in more details can refer to a few articles which expose the main recent results concerning this process (see, e.g., [29], [30]).

Collisional processes occur frequently between the small bodies of our Solar System. The best witnesses of those events are *asteroid families* in the main belt. Each family originates from the break-up of a large body, which is now represented by a group of asteroids sharing the same spectral and orbital properties (see, e.g., [20], [47]). As in the case of spin limits (Sect. 3), two regimes of collisional disruption have been defined: the *strength* regime, in which the fragmentation of the body is the only process determining the outcome (this is the case of impact experiments in laboratory), and the *gravity* regime, in which not only the fragmentation but also the gravitational interactions of fragments have an influence on their final size and velocity distributions. The transition between the two regimes has been found to occur for body sizes in the hundred meter range by numerical simulations ([3]), while the transition between the two regimes derived from the spin limits occurs at higher diameters (kilometer range; see Sect. 3 and [16]).

The first numerical simulations which reproduced successfully large scale events represented by asteroid families ([25], [26], [27], [28]), showed that when a large parent body (several tens of kilometers in diameter) is disrupted by a collision with a projectile, the generated fragments interact gravitationally during their ejections, and some of them reaccumulate to form aggregates. The final outcome of such a disruption is thus a distribution of fragments, most of the large ones being aggregates formed by gravitational reaccumulations of smaller ones. The implication of these results is that most large family members should be rubble piles and not monolithic bodies. Moreover, it was found that collisional disruptions form naturally binary systems and satellites ([25], [8]), although the timescale of their stability still needs to be determined.

The physics of the gravitational phase during which generated fragments evolve under their mutual attractions relies on the fundamental laws of classical mechanics, which are well understood. However, the development of numerical simulations which account for all the processes that may occur during this phase is a difficult task. When a large body is fragmented, the number of generated sizeable fragment can be as large as a few millions. Therefore, the numerical difficulties come from the fact that the forces must be computed for a large number of particles, up to millions, and this requires the

use of efficient numerical methods to reduce the CPU time to reasonable values. Moreover, during their evolutions, these fragments do not only evolve under distant interactions, they can also undergo physical collisions between them, which must also be dealt with. A numerical N-body code called *pkdgrav* has been developed (see [35]) to compute the evolutions of large numbers of particles. It is a parallel tree-code which is able to compute the gravitational evolutions of millions of particles and handles collisions between them. During the gravitational phase, such collisions are assumed to not cause fragmentation, but only mergers or bounces. This simplification is justified by the fact that the relative velocities between the ejected fragments are small enough that collisions between them are quite smooth. So, when collisions occur during this phase, depending on some velocity and spin criteria, the particles either merge into a single one whose mass is the sum of the particle masses and whose position is at the center of mass of the particles, or bounce with some coefficient of restitution to account for dissipation (see [26] for details). In this approximation, while the aggregates that are formed have "correct" masses, their shapes are all spherical because of the merging procedure. Of course, the final shape and spin distributions are also an important outcome of a disruption and a study is currently under way to improve the simulations: instead of merging into a single spherical particle, colliding particles will be able to stick together using rigid body approximations. Such improvement will allow the determination of the shapes and spins of aggregates formed during a catastrophic disruption.

The most poorly understood part of the collisional process is the fragmentation phase, following immediately the impact of the projectile. It usually lasts twice the time for the shock wave to propagate through the whole target (a few seconds for a kilometer-size body). The process of rock fragmentation is still a widely open area of research, relying on a large number of assumptions based on a limited number of data. Moreover, not only the physics is badly understood, the numerical techniques used to perform the computation are also confronted to some difficulties. Indeed, the fragmentation process in a rock involves two kinds of approaches, which are generally incompatible. A high-velocity impact on a rock generates a shock wave, followed by a rarefaction wave which will activate the crack propagation. Thus, the rock can be seen as a continuum for the shock treatment. On the other hand, a rock contains some discrete elements (the initial cracks). This mixture of continuum and discrete features makes the development of a numerical scheme difficult. A numerical code used to compute the fragmentation phase is generally called a *hydrocode*, which emphasizes the fact that this process involves the physics of hydrodynamics, although it occurs in a solid. Indeed, the difference between a fluid and a solid is that the deviatoric (non-diagonal) part of the stress tensor is not null in the case of a solid, while in a fluid only the spherical (diagonal) part of the stress tensor representing the pressure plays a role (see Sect. 2 for a detailed explanation of the difference between a fluid and a solid). Thus, three kinds of waves (elastic, plastic and shock) propagate through a rock during an

impact. Elastic waves are well known and determined by linear relationships between the stress and strain tensors. Plastic waves begin to develop when the material strength changes with the wave amplitude. Then, at wave amplitudes that are high enough and associated to shock waves, the body is treated as a fluid. Being non-linear, the transitory behaviors between these kinds of waves are difficult to determine analytically from constitutive models, and this probably motivated the development of numerical algorithms. The process has thus been studied by implementing the bulk properties of a given rock in a numerical model of continuous medium (a *hydrocode*), including a yielding criterion and an equation of state for the appropriate material. The main power of this method is that no assumption on the form of the stress wave that drives the fragmentation is required since the initial conditions evolve numerically based on a rheological model and a failure criterion. The appropriate regime (elastic, plastic or shock) is determined by the computation.

The 3D Lagrangian hydrocode developed by Benz and Asphaug ([2]) represents the state-of-the-art in numerical computations of dynamical fracture of brittle solids. It uses the method called Smooth Particle Hydrodynamics (SPH) (see [1] for a review of this method). Basically, the value of the different hydrodynamics quantities are known at finite numbers of points which move with the flow. Starting from a spatial distribution of these points called particles, the SPH technique allows to compute the spatial derivatives without the necessity of an underlying grid. The 3D SPH hydrocode is thus able to simulate consistently from statistical and hydrodynamical points of view the fragments that are smaller or larger than the chosen resolution (number of SPH particles). The resulting system has proven to predict successfully the sizes, positions and velocities of fragments measured in laboratory experiments, without requiring the adjustment of too many free parameters ([2]); moreover, associated with the N-body code *pkdgrav*, it has successfully reproduced the main properties of asteroid families ([25], [26], [27], [28]).

For the sake of completeness, we recall here the basic equations that must be solved to compute the fragmentation process. Other important concepts, such as the equations of state, the model of brittle failure used to propagate damage and the method to distribute appropriately incipient flaws in the modeled rock with a Weibull distribution are not reproduced here, as they have been described several times (see [2], [30]).

The basic equations that must be solved to compute the process are the well-known conservation equations of hydrodynamics that can be found in standard textbooks. The first equation represents the mass conservation. Its expression is:

$$\frac{d\rho}{dt} + \rho \frac{\partial}{\partial x_\alpha} v_\alpha = 0 \quad (22)$$

where d/dt is the lagrangian time derivative. Other variables have their usual meaning (i.e. ρ is the bulk density, v is the velocity and x the posi-

tion) and the usual summation rule over repeated indices is used. The second equation describes the momentum conservation (in absence of gravity):

$$\frac{dv_\alpha}{dt} = \frac{1}{\rho} \frac{\partial}{\partial x_\beta} \sigma_{\alpha\beta} \quad (23)$$

where $\sigma_{\alpha\beta}$ is the stress tensor given by:

$$\sigma_{\alpha\beta} = -P\delta_{\alpha\beta} + S_{\alpha\beta} \quad (24)$$

where P is the isotropic pressure and $S_{\alpha\beta}$ is the traceless deviatoric stress tensor. The energy conservation is then expressed by the equation:

$$\frac{du}{dt} = -\frac{P}{\rho} \frac{\partial}{\partial x_\alpha} v_\alpha + \frac{1}{\rho} S_{\alpha\beta} \dot{\epsilon}_{\alpha\beta} \quad (25)$$

where $\dot{\epsilon}_{\alpha\beta}$ is the strain rate tensor given by:

$$\dot{\epsilon}_{\alpha\beta} = \frac{1}{2} \left(\frac{\partial}{\partial x_\beta} v_\alpha + \frac{\partial}{\partial x_\alpha} v_\beta \right). \quad (26)$$

This set of equations is still insufficient in the case of a solid since the evolution in time of $S_{\alpha\beta}$ must be specified. The basic Hooke's law model is assumed in which the stress deviator rate is proportional to the strain rate:

$$\frac{dS_{\alpha\beta}}{dt} = 2\mu \left(\dot{\epsilon}_{\alpha\beta} - \frac{1}{3} \delta_{\alpha\beta} \dot{\epsilon}_{\gamma\gamma} \right) + S_{\alpha\gamma} R_{\beta\gamma} + S_{\beta\gamma} R_{\alpha\gamma} \quad (27)$$

where μ is the shear modulus and $R_{\alpha\beta}$ is the rotation rate tensor given by:

$$R_{\alpha\beta} = \frac{1}{2} \left(\frac{\partial}{\partial x_\beta} v_\alpha - \frac{\partial}{\partial x_\alpha} v_\beta \right). \quad (28)$$

This term allows the transformation of the stresses from the reference frame associated with the material to the laboratory reference frame in which the other equations are specified.

This set of equations can now be solved, provided an equation of state is specified, $P = P(\rho, u)$, linking the pressure P to the density ρ and internal energy u . The Tillotson equation of state for solid material ([42]) is generally used. Its expression and method of computation, as well as parameters for a wide variety of rocks are described in [23] (Appendix II). Other equations of states have been developed and all have different pros and cons and remain necessarily limited to materials studied in laboratory. This is one of the limits of any collisional model that necessarily relies on the behavior of known materials that do not necessarily represent the materials constituting an asteroid.

Perfectly elastic materials are well described by these equations. Plastic behavior beyond the Hugoniot elastic limit is introduced in these relations by using the von Mises yielding criterion (see Sect. 2). This criterion limits the deviatoric stress tensor to:

$$S_{\alpha\beta} = f S_{\alpha\beta} \quad (29)$$

where f is computed from:

$$f = \min\left[\frac{Y_0^2}{3J_2}, 1\right], \quad (30)$$

where J_2 is the second invariant of the deviatoric stress tensor (see Sect. 2) and Y_0 is a material dependent yielding stress which generally depends on temperature, density, etc. in such a way that it decreases with increasing temperature until it vanishes beyond the melting point.

The von Mises criterion is adapted to describe the failure of ductile media such as metals. Brittle materials like rocks do not undergo a plastic failure but rather “break” if the applied stresses exceed a given threshold. Conversely, the yielding beyond the Hugoniot elastic limit does not prescribe any permanent change in the constitution of the material, since once stresses are reduced the original material remains behind, possibly heated by the motion against the remaining stress, but otherwise not weakened. Therefore, it is not adapted to impacts into rocks, as any yielding beyond the elastic limit invariably involves irreversible damage, and one needs to know how the rock is permanently altered by the event. A realistic fracture model is then clearly required to study the disruption of a solid body. The Grady-Kipp model of brittle failure is generally the model implemented in numerical codes aimed at simulating fragmentation processes in solid bodies ([10]).

Despite these recent successes of impact simulations to reproduce some experiments and asteroid family properties, there are still many issues and uncertainties in the treatment of the fragmentation phase. Some of the important ones are:

- **Material parameters:** one of the main limitations of all researches devoted to the fragmentation process comes from the uncertainties on the material properties of the objects involved in the event. For instance, ten material parameters describe the usually adopted Tillotson equation of state (see e.g. [23], appendix II). Other sensitive material-dependent parameters are, for instance, the shear and bulk modulus, but the most problematic parameters are probably the two Weibull parameters m and k used to characterize the distribution of initial cracks in the target. In fact, as already mentioned (Sect. 2.3), data are still scarce about these parameters, due to the experimental difficulty to determine their values. This is a crucial problem because so far, the validation of numerical simulations by confrontation to experiments has been done by choosing freely those missing values so as to match the experiments ([2]). This is not a totally satisfactory approach for an *ab initio* method such as the one provided by SPH simulations. Unfortunately, this is often the only alternative which one has. A database including both the material parameters of targets and

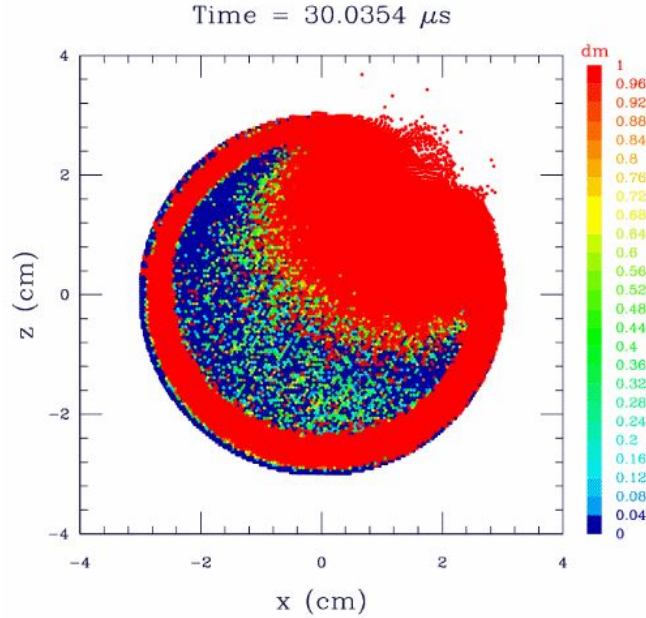


Fig. 4. SPH simulation of the impact of a projectile on a basalt target in the same conditions as a high-velocity experiment ([32]). The plot shows how damage (labelled dm) propagated $30 \mu s$ after the impact (red zones are fully damaged). In particular, a core fragment can be identified which has the same mass and velocity as the one measured in the experiment.

outcomes of impact experiments using these targets is thus required to perform a full validation of numerical codes. Such a project has started using the experimental expertise of japanese researchers from Kobe University, and the numerical expertise of french and swiss researchers from Côte d’Azur Observatory and Berne University. For instance, measurements of Weibull parameters of a Yakuno basalt used in impact experiments were made in this purpose ([33]).

- **Crack propagation speed in a solid:** the value of the crack growth speed is usually assumed to be 40% of the longitudinal sound speed in numerical simulations. This speed highly influences the number of cracks that can be activated for a given strain rate (see Sect. 2.3). It thus plays a major role in the number and sizes of fragments which are eventually created. The lack of measurements of this speed and its possible dependency on material type leave no choice but to use an intermediate value such as the one currently assumed. However, it is important to keep in mind that this may need to be revised once some cracks are found to propagate at higher/lower speed in a sufficient number of experiments.

- **Model of fragmentation:** up to now, all published simulations of impact disruption have been done using in general the Grady-Kipp model of brittle failure ([10]. In this model, damage increases as a result of crack activation, and microporosity (pore crushing, compaction) is not treated. However, several materials contain a certain degree of porosity (e.g. pumice, gypsum), and asteroids belonging to dark taxonomic types (e.g. C, D) are believed to contain a high level of microporosity. The behavior of a porous material subjected to an impact is likely to be different than the behavior of a non-porous one, as already indicated by some experiments (e.g. [19]). Therefore, a model for porous materials is required, in order to be able to address the problem of dark-type asteroid family formations, and to characterize the impact response of porous bodies in general (including porous planetesimals during the phase of planetary growth). Such models have been developed recently and inserted in numerical codes ([46], [4]). However, so far their application has been limited to the cratering regime and their validity is still not guaranteed. Moreover, it will be important to check their validity in the disruptive regime by comparison to impact experiments, such as recent ones made on pumice by the group of Kobe led by A. Nakamura.
- **Rotating targets:** all simulations of catastrophic disruption have been performed starting with a non-rotating target. However, in the real world, small bodies are spinning (see Sect. 3), and the effect of the rotation on the fragmentation is totally unknown. Some preliminary experiments have been performed suggesting that, everything else being equal, a rotating target is easier to disrupt than a non-rotating one (K. Housen, private communication). If this is confirmed, this will be an important result as all models of collisional evolutions of small body populations use prescriptions that are provided by numerical simulations on non-rotating targets. In particular, the lifetime of small bodies may be shorter than expected if their rotation has an effect on their ability to survive collisions. It will thus be important to characterize the impact response of rotating bodies, both experimentally and numerically, although on both sides, starting with a rotating body is confronted to several difficulties.

6 Conclusion

Our understanding of the disruption mechanisms of small bodies of our Solar System has greatly improved in the last decades, thanks to the development of analytical theories and sophisticated simulations. However, there are still many uncertainties, and problems that need to be investigated. Concerning the spin limits and tidal disruptions, the theories that have been developed so far are all static. Nevertheless, they allowed us to understand that the spin barrier observed for large asteroids does not imply necessarily that these bodies are pure rubble piles, in contrast with the usual interpretation. On the

other hand, the small fast rotators do not need to have much cohesion to spin at such high rates (see Sect. 3). Then, these theories allowed us to revisit the concept of Roche limit for solid ellipsoidal bodies with and without cohesion. They showed that, contrary to a fluid, a solid body can come much closer to a planet or a primary and with a wide variety of shapes (see Sect. 4). However, these theories rely on a model of material strength (Drucker-Prager or Mohr-Coulomb) which is not necessarily unique and they are limited to bodies whose shapes are idealized ellipsoids. Some other strength models or non-idealized shapes should certainly be considered. Then, a complete dynamical investigation of these problems is required to determine the outcome of rotational and tidal break-ups of small bodies.

Sophisticated numerical codes have been developed to study the process of impact disruption of a small body. The outcome of some impact experiments and the main properties of some asteroid families have been reproduced successfully with one of those codes, based on the Smooth Particle Hydrodynamics technique and the Grady-Kipp model of brittle failure. However, as discussed in Sect. 5, there are still many issues, and the road is still long before being able to characterize with high accuracy the impact response of a small body as a function of its material properties. This is a challenging topic which has many applications. Indeed, the collisional process plays a fundamental role in the different phases of the history of our Solar System, from the phase of planetary growth by collisional accretion to the current phase during which small bodies are catastrophically disrupted. Moreover, the determination of the impact response of a small body as a function of its physical properties is crucial in the definition of efficient mitigation strategies aimed at deflecting a potential threatening near-Earth asteroid whose trajectory leads it to the Earth.

Thus, researches devoted to these disruption mechanisms and to the concept of strength will certainly keep busy future generations of researchers, and they will also take advantage of future space missions devoted to in-situ investigations and sample returns from small bodies.

References

1. W. Benz: *Smooth Particle Hydrodynamics - A Review*. In: Proceedings of the NATO Advanced Research Workshop on The Numerical Modelling of Nonlinear Stellar Pulsations Problems and Prospects, ed. by J. Robert Buchler (Kluwer Academic Publishers, Dordrecht, 1990).
2. W. Benz, and E. Asphaug: *Impact simulations with fracture. I- Method and tests*, Icarus **107**, 98 (1994)
3. W. Benz, and E. Asphaug: *Catastrophic disruptions revisited*, Icarus **142**, 5 (1999)
4. W. Benz, and M. Jutzi: *Collision and impact simulations including porosity*. In: Nearth-Earth Objects, our celestial neighbors: Opportunity and Risks, ed. by A.

- Milani, G.B. Valsecchi and D. Vokrouhlicky, IAU Symposium 236 (IAU, 2007) in press
5. W.F. Bottke, A. Morbidelli, R. Jedicke, J.M. Petit, H. Levison, P. Michel, and T.S. Metcalfe: *Debiased orbital and absolute magnitude distribution of the Near-Earth Object population*, Icarus **156** 399 (2002)
 6. S. Chandrasekhar: *Ellipsoidal Figures of Equilibrium* (Dover, New York, 1969)
 7. W.F. Chen, and D.J. Han: *Plasticity for Structural Engineers* (Springer, Berlin and New-York, 1988)
 8. D.D. Durda, W.F. Bottke, B.L. Enke, W.J. Merline, E. Asphaug, D.C. Richardson, Z.M. Lehnardt: *The formation of asteroid satellites in large impacts: results from numerical simulations*, Icarus **170**, 243 (2004)
 9. B.J. Gladman, F. Migliorini, A. Morbidelli, V. Zappalà, P. Michel, A. Cellino, Ch. Froeschlé, H.F. Levison, M. Bailey, and M. Duncan: *Dynamical lifetimes of objects injected into asteroid belt resonances*, Science **277**, 197 (1997)
 10. D.E. Grady, and M.E. Kipp: *Continuum modeling of explosive fracture in oil shale*, Int. J. Rock Mech. Min. Sci. Geomech. Abstr. **17**, 147 (1980)
 11. A.W. Harris: *The rotation rates of very small asteroids: Evidence for "rubble pile" structure*, Lunar Planet. Sci. **27**, 493 (1996)
 12. K.A. Holsapple: *Equilibrium configurations of solid ellipsoidal cohesionless bodies*, Icarus **154**, 432 (2001)
 13. K.A. Holsapple, I. Glibin, K.R. Housen, A. Nakamura, and E. Ryan: *Asteroid impacts: Laboratory experiments and scaling laws*. In: Asteroids III, ed. by W.F. Bottke, A. Cellino, P. Paolicchi, and R.P. Binzel (University of Arizona Press, Tucson, 2002) pp. 443-462.
 14. K.A. Holsapple: *Equilibrium figures of spinning bodies with self-gravity*, Icarus **172**, 272 (2004)
 15. K.A. Holsapple, and P. Michel: *Tidal disruptions: a continuum theory for solid bodies*, Icarus **183**, 331 (2006)
 16. K.A. Holsapple: *Spin limits of Solar System bodies: From the small fast-rotators to 2003 EL61*, Icarus **187**, 500 (2007)
 17. K.A. Holsapple: *Spinning rods, elliptical disks and solid ellipsoidal bodies: Elastic and plastic stresses and limit spins*, submitted (2007)
 18. K.A. Holsapple, and P. Michel: *Tidal disruption II: a continuum theory for solid bodies with strength, with applications to the satellites of our Solar System*, Icarus, submitted (2007)
 19. K.R. Housen, and K.A. Holsapple: *Scale effects in strength-dominated collisions of rocky asteroids*, Icarus **142**, 21 (1999)
 20. Z. Knežević, A. Lemaître, and A. Milani: *The determination of asteroid proper elements*. In: Asteroids III, ed. by W.F. Bottke, A. Cellino, P. Paolicchi, and R.P. Binzel (University of Arizona Press, Tucson, 2002) pp. 603-612.
 21. J.H. Jeans: *The motion of tidally-distorted masses, with special reference to the theories of cosmogony*, Mem. Roy. Astron. Soc. London **62**, 1 (1917)
 22. S.C. Lowry, et al.: *Direct detection of the asteroidal YORP effect*, Science **316**, 272 (2007)
 23. H.J. Melosh: *Impact cratering: a geologic process* (Oxford University Press, New York, 1989).
 24. H.J. Melosh, E.V. Ryan, and E. Asphaug: J. Geophys. Res. **97**, 14735 (1992)
 25. P. Michel, W. Benz, P. Tanga, and D.C. Richardson: *Collisions and gravitational reaccumulations: forming asteroid families and satellites*, Science **294**, 1696 (2001)

26. P. Michel, W. Benz, P. Tanga, and D.C. Richardson: *Formation of asteroid families by catastrophic disruption: simulations with fragmentation and gravitational reaccumulation*, *Icarus* **160**, 10 (2002)
27. P. Michel, W. Benz, and D.C. Richardson: *Fragmented parent bodies as the origin of asteroid families*, *Nature* **421**, 608 (2003)
28. P. Michel, W. Benz, and D.C. Richardson: *Disruption of pre-shattered parent bodies*, *Icarus* **168**, 420 (2004)
29. P. Michel, W. Benz, and D.C. Richardson: *Catastrophic disruption and family formation: a review of numerical simulations including both fragmentation and gravitational reaccumulation*, *Planet. Space Sci.* **52**, 1109 (2004)
30. P. Michel: *Modelling collisions between asteroids: from laboratory experiments to numerical simulations*. In: *Dynamics of Extended Celestial Bodies*, ed. by J. Souchay, *Lecture Notes in Physics* (Springer, Berlin, 2006), pp. 117-143.
31. P. Michel, and K.A. Holsapple: *Tidal disturbances of small cohesionless bodies: limit on planetary close approach distances*. In: *Near-Earth Objects, our celestial neighbors: Opportunity and Risks*, ed. by A. Milani, G.B. Valsecchi and D. Vokrouhlický, *IAU Symposium 236* (IAU, 2007) in press
32. A. Nakamura, and A. Fujiwara: *Velocity distribution of fragments formed in a simulated collisional disruption*, *Icarus* **92**, 132 (1991)
33. A.M. Nakamura, P. Michel, and M. Seto: *Weibull parameters of Yakuno basalt targets used in documented high-velocity impact experiments*, *J. Geophys. Res.* **112**, E02001, doi:10.1029/2006JE002757 (2007)
34. D.C. Richardson, W.F. Bottke, and S.G. Love: *Tidal distortion and disruption of Earth-crossing asteroids*, *Icarus* **134**, 47 (1998)
35. D.C. Richardson, T. Quinn, J. Stadel, and G. Lake: *Direct large-scale N-body simulations of planetesimal dynamics*, *Icarus* **143**, 45 (2000)
36. D.C. Richardson, Z.M. Leinhardt, W.F. Bottke, H.J. Melosh, and E. Asphaug: *Gravitational aggregates: Evidence and evolution*. In: *Asteroids III*, ed. by W.F. Bottke, A. Cellino, P. Paolicchi, and R.P. Binzel (University of Arizona Press, Tucson, 2002), pp. 501-515.
37. D.C. Richardson, P. Elankumaran, and R. Sanderson: *Numerical experiments with rubble piles: equilibrium shapes and spins*, *Icarus* **173**, 349 (2005)
38. E.A. Roche: *Acad. Sci. Lett. Montpellier. Mem. Section Sci.* **1**, 243 (1847)
39. I. Sharma, J.T. Jenkins, and J.A. Burns: *Tidal encounters of ellipsoidal granular asteroids with planets*, *Icarus* **183**, 312 (2006)
40. D.J. Scheeres, S.J. Ostro, R.A. Werner, E. Asphaug, and R.S. Hudson: *Effect of gravitational interactions on asteroid spin states*, *Icarus* **147**, 106 (2000)
41. D.J. Scheeres: *Changes in rotational angular momentum due to gravitational interactions between two finite bodies*, *Celest. Mech. Dynam. Astron.* **81**, 39 (2001).
42. J.H. Tillotson: *Metallic equations of state for hypervelocity impact*, *General Atomic Report GA-3216*, July (1962).
43. D. Vokrouhlický, and D. Capek: *YORP-induced long-term evolution of the spin state of small asteroids and meteoroids: RubbinCam's approximation*, *Icarus* **159**, 449 (2002)
44. K.J. Walsh, and D.C. Richardson: *Binary near-Earth asteroid formation: Rubble pile model of tidal disruptions*, *Icarus* **180**, 201 (2006)
45. W.A. Weibull: *Ingvetensk. Akad. Handl.* **151**, 5 (1939)
46. K. Wuennemann, G.S. Collins, and H.J. Melosh: *A strain-based porosity model for use in hydrocode simulations of impacts and implications for transient crater growth in porous targets*, *Icarus* **180**, 514 (2006)

47. V. Zappalà, A. Cellino, A. Dell'Oro, and P. Paolicchi: *Physical and dynamical properties of asteroid families*. In: Asteroids III, ed. by W.F. Bottke, A. Cellino, P. Paolicchi, and R.P. Binzel (University of Arizona Press, Tucson, 2002), pp. 619-631.

To be published in:
"Small Bodies in Planetary Systems".
(Mann, Nakamura, Mukai eds.)
Submitted to Lecture Notes in Physics series by Springer
Funded by the 21st Century COE Program
"Origin and Evolution of Planetary Systems"

Index

- aggregate, 21
- angle of friction, 5
- asteroid families, 21
- average stresses, 12

- body forces, 16
- brittle material, 25

- catastrophic disruption, 21
- cohesion, 5
- cohesionless, 4
- compressive strength, 4

- deviatoric stress tensor, 24
- Drucker-Prager criterion, 5
- dynamic strength, 9

- elastic limit, 4
- elastic wave, 23
- equation of state, 24

- failure criterion, 4
- fragmentation phase, 22

- Grady-Kipp model, 25
- gravitational reaccumulation, 21

- Hooke's law, 24
- hydrocode, 22

- incipient flaws, 8

- Jean's problem, 18

- limit states, 11

- microporosity, 27
- Mohr-Coulomb criterion, 5

- plastic wave, 23
- porous material, 27

- Roche limit, 14

- shear modulus, 24
- shear strength, 4
- shock wave, 23
- Smooth Particle Hydrodynamics, 23
- spin limits, 10
- spin-locked, 17
- static strength, 9
- static theory, 17
- strain rate tensor, 24
- stray body, 17
- strength, 3
- stress equilibrium equations, 15

- tensile strength, 4
- tidal disruption, 14
- tidal forces, 15
- Tillotson equation, 24
- Tresca criterion, 5

- Von Mises criterion, 5

- Weibull distribution, 8
- Weibull parameters, 8